BIOCHEMISTRY
including biophysical chemistry & molecular biology

Article

pubs.acs.org/biochemistry

Nickel Superoxide Dismutase: Structural and Functional Roles of His1 and Its H-Bonding Network

Kelly C. Ryan,[†] Abigail I. Guce,[†] Olivia E. Johnson,[§] Thomas C. Brunold,[§] Diane E. Cabelli,[∥] Scott C. Garman,[‡] and Michael J. Maroney*[,†]

[†]Department of Chemistry, University of Massachusetts at Amherst, 104 Lederle Graduate Research Tower A, 710 North Pleasant Street, Amherst, Massachusetts 01003, United States

[‡]Department of Biochemistry and Molecular Biology, University of Massachusetts at Amherst, 913 Lederle Graduate Research Tower A, 710 North Pleasant Street, Amherst, Massachusetts 01003, United States

[§]Department of Chemistry, University of Wisconsin—Madison, 1101 University Avenue, Madison, Wisconsin 53706, United States

[∥]Department of Chemistry, Brookhaven National Laboratory, Building 555A, P.O. Box 5000, Upton, New York 11973, United States

Supporting Information

ABSTRACT: Crystal structures of nickel-dependent superoxide dismutases (NiSODs) reveal the presence of a H-bonding network formed between the NH group of the apical imidazole ligand from His1 and the Glu17 carboxylate from a neighboring subunit in the hexameric enzyme. This interaction is supported by another intrasubunit H-bond between Glu17 and Arg47. In this study, four mutant NiSOD proteins were produced to experimentally evaluate the roles of this H-bonding network and compare the results with prior predictions from density functional theory calculations. The X-ray crystal structure of H1A-NiSOD, which lacks the apical ligand entirely, reveals that in the absence of the Glu17−His1 H-bond, the active site is disordered. Characterization of this variant using X-ray absorption spectroscopy (XAS) shows that Ni(II) is bound in the expected N_2S_2 planar coordination site. Despite these structural perturbations, the H1A-NiSOD variant retains 4% of wild-type (WT) NiSOD activity. Three other mutations were designed to preserve the apical imidazole ligand but perturb the H-bonding network: R47A-NiSOD, which lacks the intramolecular H-bonding interaction; E17R/R47A-NiSOD, which retains the intramolecular H-bond but lacks the intermolecular Glu17−His1 H-bond; and E17A/R47A-NiSOD, which lacks both H-bonding interactions. These variants were characterized by a combination of techniques, including XAS to probe the nickel site structure, kinetic studies employing pulse-radiolytic production of superoxide, and electron paramagnetic resonance to assess the Ni redox activity. The results indicate that in addition to the roles in redox tuning suggested on the basis of previous computational studies, the Glu17−His1 H-bond plays an important structural role in the proper folding of the "Ni-hook" motif that is a critical feature of the active site.

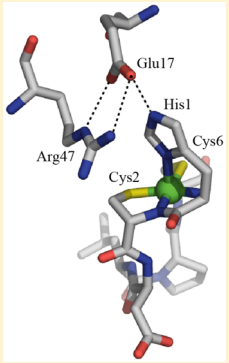

Superoxide dismutases (SODs) are metalloenzymes that protect aerobic organisms from oxidative stress caused by the superoxide anion radical ($O_2^{\bullet-}$) and its reaction products.[1−4] Elimination of superoxide is achieved by catalyzing its disproportionation reaction to produce molecular oxygen (O_2) and hydrogen peroxide (H_2O_2) at rates approaching the diffusion limit. The catalysis proceeds by a "ping-pong" mechanism in which the redox active metal cofactor cycles between oxidized and reduced states that differ by one electron (eqs 1−3).

$$M^{n+1} + O_2^{\bullet-} \rightarrow M^{n+} + O_2 \quad (1)$$

$$M^{n+} + O_2^{\bullet-} + 2H^+ \rightarrow M^{n+1} + H_2O_2 \quad (2)$$

$$2O_2^{\bullet-} + 2H^+ \rightarrow O_2 + H_2O_2 \quad (3)$$

Three classes of SODs are based on amino acid sequence homology: CuZnSOD, FeSOD and MnSOD, and NiSOD. Like the Fe- and MnSODs, the more recently discovered NiSOD enzyme catalyzes the disproportionation of $O_2^{\bullet-}$ by cycling between M(III) and M(II) oxidation states.[5] The CuZnSOD, FeSOD, and MnSOD proteins bind their respective catalytic metal cofactors using exclusively N/O-donor ligands (Figure 1).[6−8] In contrast, NiSOD employs cysteine thiolate ligation to bring the Ni(III/II) couple into a range relevant for SOD catalysis (~300 mV).[4] In the reduced state of NiSOD, the Ni(II) cofactor adopts a four-coordinate planar geometry that features two thiolate ligands (Cys2 and Cys6), the N-terminal amine from His1, and a deprotonated amide from the Cys2 backbone.[9,10] In the oxidized state of NiSOD, the Ni(III) ion additionally binds the imidazole side chain of His1 via the N_δ donor atom, which results in a five-coordinate pyramidal geometry around the nickel ion with the His1 imidazole at the apex (Figure 1).[9,10]

The high-resolution crystal structures of wild-type (WT) NiSOD from *Streptomyces seoulensis* and *Streptomyces coelicolor*

Received: October 5, 2014
Revised: January 8, 2015
Published: January 12, 2015

© 2015 American Chemical Society

DOI: 10.1021/bi501258u
Biochemistry 2015, 54, 1016−1027

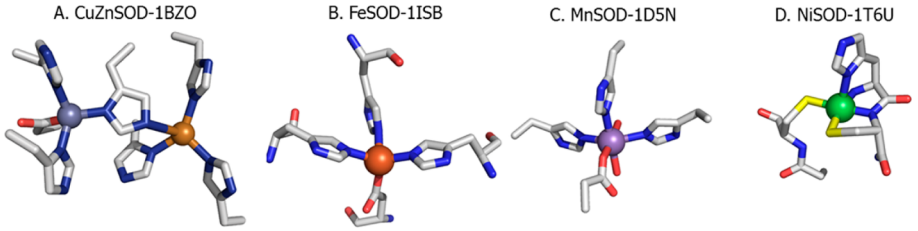

Figure 1. Active sites of (A) CuZnSOD, (B) FeSOD, (C) MnSOD, and (D) NiSOD.

also show that NiSOD forms a homohexamer comprised of four-helix bundle monomers that place the nickel sites in a roughly octahedral arrangement ~25 Å apart. The hexameric quaternary structure can be viewed as a dimer of trimers (Figure 2) where three monomer subunits are arranged like the

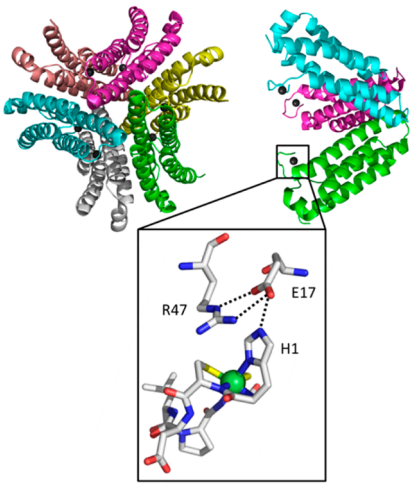

Figure 2. Overall hexamer (top left, looking down the three-fold axis) and trimer (top right, perpendicular to the three-fold axis) protein oligomeric state(s), and active site of NiSOD shown in the His-on, Ni(III)-bound state and H-bonding interactions from Glu17 and Arg47 (Protein Data Bank entry 1T6U).

legs of a tripod and two trimers interdigitate to form the hexamer. The hexamer is stabilized by hydrophobic, salt bridge, and H-bonding interactions. One important intersubunit interaction involves a H-bonding network formed between the NH group of the apical imidazole ligand from His1 and the Glu17 carboxylate from a neighboring subunit. This interaction is further supported by an intrasubunit H-bond between Glu17 and Arg47 (Figure 2). The crystal structures also reveal that the His1 side chain is disordered in the resting state of the enzyme, resulting in a hexamer that contains active sites that are a mixture of Ni(III)/His_{on} and Ni(II)/His_{off} forms, but where the His1−Glu17 H-bond is maintained in both structures.[9,10]

Density functional theory (DFT) computations have been used to investigate the role of the His1−Glu17−Arg47 H-bonding network in stabilizing the Ni(III)/His_{on} conformation of NiSOD, as well as its role in influencing the interaction between the His1 imidazole and the nickel cofactor.[11] Using the information from the crystal structures, five computational models were constructed and subjected to DFT energy minimizations: **ox**$^{1-3}$, **ox-His**$_{off}$, and **red**. In the **ox**^{2} and **ox**^{3} models of Ni(III)SOD, the H-bonding interactions between His1 and Glu17 (**ox**^{3}) and additionally those between Arg47 and Glu17 (**ox**^{2}) were included. The results obtained indicated that the H-bonding interactions are important in adjusting the Ni−N_{δ}His1 distance, and thus in tuning the energy of the redox active molecular orbital (Ni $3d_{z^2}$) and thereby adjusting the redox potential of the active site.[11] In addition, the results obtained for a model that contains Ni(II) and lacks the axial imidazole ligand (**red**), and one that includes Ni(III) and the His1 imidazole in a nonbonding position that maintains the H-bond with Glu17 in the C_2-related subunit (**ox-His**$_{off}$), indicated that the His1 imidazole side chain is also involved in stabilizing the Ni(III) state of NiSOD and in promoting metal-centered rather than ligand (thiolate)-centered redox chemistry.[11]

In the study presented here, we have used an experimental approach employing site-directed mutagenesis to generate four *S. coelicolor* NiSOD mutant proteins to probe the roles of the His1−Glu17−Arg47 H-bonding network and test the predictions from the calculations. The four variants are H1A-NiSOD, which lacks the apical imidazole and associated H-bond with Glu17; R47A-NiSOD, which retains the intersubunit Glu17−His1 H-bond but lacks the Arg47−Glu17 interaction; E17R/R47E-NiSOD, which retains the intrasubunit Glu17−Arg47 H-bond but lacks the intersubunit interaction between Glu17 and His1; and E17A/R47A-NiSOD, which lacks all of these H-bonding interactions. The results of these studies are compared with those obtained for recombinant *S. coelicolor* WT-NiSOD and largely confirm the predictions from the calculations. All of the mutant proteins have impaired catalytic activity and are isolated primarily in the Ni(II) oxidation state. In addition, a crystal structure of the H1A-NiSOD variant shows a disordered active site, implying that the active site does not properly fold in the absence of the His1−Glu17 H-bonding interaction and demonstrating a critical structural role for the His1−Glu17 H-bond. Collectively, our results indicate that both the presence of His1 and the His1−Glu17−Arg47 H-bonding network are critical features for the proper organization of the active site and for supporting redox catalysis.

MATERIALS AND METHODS

Site-Directed Mutagenesis. The H1A-NiSOD mutant plasmid was prepared by polymerase chain reaction (PCR) of the WT *S. coelicolor* NiSOD gene (*sodN*) with a mutagenic 5′-primer and 3′-SODNU (Table SI-1 of the Supporting Information). The PCR product was gel purified (1% agarose) and treated with T4 DNA polymerase to create overhangs complementary to the ligation-independent cloning (LIC) vector pET30 Xa/LIC (Novagen). The insert was annealed to the vector, and NovaBlue (Novagen) competent cells were transformed with the pET30 Xa/LIC plasmid containing the *sodN* mutant gene for selection. The plasmids containing mutagenic *sodN* were isolated using a plasmid mini prep kit (Qiagen), and DNA sequencing was performed to confirm the

DOI: 10.1021/bi501258u
Biochemistry 2015, 54, 1016−1027

Table 1. Characterization of Native, WT, H1A, and H-Bonding Variants of NiSOD

NiSOD sample	MW (ESI-MS) (calcd value)	quaternary structure (ESI-MS)	Ni/protein	kinetics, k_{cat} at pH 7.5 ($\times 10^9$ M^{-1} s^{-1})	T_m (°C)
native (*S. seoulensis*)	13192.5 (13189.1)	hexamer	0.74	1.18	88.0[b] (>80)
WT	18171.2[a] (18169.6)	hexamer	0.88	0.55	84.8,[b] 65.2[c]
H1A-NiSOD	18130.9[a] (18103.3)	hexamer	0.19	0.047	77.8[b]
R47A-NiSOD	18084.0[a] (18084.3)	hexamer	0.60	0.121	76.4[b]
E17A/R47A-NiSOD	18025.1[a] (18026.2)	hexamer	0.86	0.036	68.5[b]
E17R/R47E-NiSOD	18168.6[a] (18169.4)	hexamer	0.29	0.095	67.5[b]

[a]Determined for the expressed fusion protein. [b]Heat capacity peak maximum. [c]Heat capacity shoulder, BDL (below the detectable limit of the assay).

expected base sequence for the mutant (University of Massachusetts at Amherst DNA sequencing facility).

The R47A-NiSOD mutant plasmid was prepared by PCR of the WT-NiSOD pET-30 Xa/LIC plasmid with mutagenic 5′- and 3′-primers, and the E17A/R47A-NiSOD and E17R/R47E-NiSOD double mutations were generated by PCR of the R47A-NiSOD pET-30 Xa/LIC plasmid with mutagenic 5′- and 3′-primers using the QuikChange XL site-directed mutagenesis kit (Table SI-1 of the Supporting Information). NovaBlue (Novagen) competent cells were transformed with the PCR products and selected for mutant plasmids. The plasmids containing mutagenic *sodN* were isolated using a plasmid mini prep kit (Qiagen), and DNA sequencing was performed to confirm the expected base sequences for the mutants (W. M. Keck DNA facility at Yale University, New Haven, CT). BL21(DE3) pLysS (Novagen) competent cells were transformed with the plasmid containing the desired mutation(s), and the variant protein was expressed and purified as previously described[12,13] and detailed below.

Expression, Purification, Processing, and Reconstitution of Mutant Proteins. The H1A-NiSOD and R47A-NiSOD proteins were expressed and purified as previously reported.[12−14] Single colonies were grown overnight at 37 °C while being shaken in 10 mL of Luria-Bertani broth, supplemented with chloramphenicol (cam) and kanamycin (kan) for selection. These cultures were added to 1 L of prewarmed fresh medium, grown to an OD_{600} of 0.6, and then induced with 0.8 mM isopropyl β-D-1-thiogalactopyranoside (IPTG) for 3−5 h. Cells were harvested by centrifugation, resuspended in 40 mL of Ni-NTA binding buffer [10 mM imidazole, 50 mM sodium phosphate, and 300 mM sodium chloride (pH 8.0)], and then frozen at −80 °C to lyse the cells. A low level of soluble protein expression was observed for E17A/R47A-NiSOD and E17R/R47E-NiSOD using the previously reported expression protocol, and inclusion bodies were observed in the cell pellet when an induction temperature of 37 °C was used for expression. Therefore, these mutant proteins were expressed at an induction temperature of 28 °C, and cells were harvested after 12−14 h and resuspended as described above. The cell harvests were thawed and treated with 100 μL of a DNase I solution [10 mg/mL DNase I, 10 mM magnesium chloride, 20 mM Tris (pH 7.5), and 40% glycerol] at 37 °C until the viscosity of the solution was significantly reduced. The cell lysate was centrifuged for 5 min at 8000 rpm, and the supernatant was used for protein purification.

All chromatographic purifications employed an AKTA-FPLC system (Amersham Biosciences). The cell lysate supernatant was loaded onto a column (Pharmacia HR10) containing Ni-NTA HisBind Superflow resin (Novagen) at a rate of 3 mL/min with Ni-NTA binding buffer. Once the absorbance at 280 nm returned to the baseline value, the buffer was changed to 12% elute buffer [250 mM imidazole, 50 mM Tris, and 300 mM sodium chloride (pH 8.0)] in one step, and the column was washed with 7 column volumes of 12% elute buffer. The fusion protein was then eluted from the column using 70% elute buffer. Electrospray ionization mass spectrometry (ESI-MS) was used to confirm the molecular weight (MW) of the expected fusion protein (*vide infra*).

To remove imidazole from the protein sample, the fusion protein was loaded onto a column (Pharmacia HR10) containing Q-Sepharose resin at a rate of 3 mL/min with bind buffer [50 mM Tris (pH 8.50)]. Once the absorbance at 280 nm returned to the baseline value, the buffer was changed to 40% elute buffer [50 mM Tris and 500 mM sodium chloride (pH 8.5)] in one step, and the fusion protein was then eluted from the column and collected. The eluted sample was adjusted to factor Xa buffer conditions [5 mM $CaCl_2$, 50 mM Tris, and 100 mM NaCl (pH 8.0)] for cleavage of the N-terminal fusion peptide with factor Xa (EMD). The concentration of fusion protein in factor Xa cleavage buffer was determined using a bicinchoninic acid (BCA) assay. The assay was performed using the Enhanced Test Tube Protocol outlined in Pierce's BCA Protein Assay Kit instruction manual. Factor Xa was then added to the protein sample (30 μL of 2.1 units/μL factor Xa/50 mg of fusion protein), and the mixture was incubated at 4 °C. The extent of cleavage was monitored using 16% SDS−PAGE. Processed protein was reduced with a 5-fold excess of dithiothreitol (DTT) and reconstituted with a 3-fold excess of $NiCl_2$ in an anaerobic glovebox (Coy Laboratory Products, Inc.). Excess DTT and Ni were removed by the same FPLC purification protocol utilized to remove imidazole in the procedure described above.

A nickel-loaded sample of H1A-NiSOD was incubated with a 15-fold excess of imidazole in an anaerobic glovebox (Coy Laboratory Products, Inc.) for 2 h. Excess imidazole was removed using a 10 kDa centrifugal concentrator (Vivaspin 500). The imidazole-treated sample of H1A-NiSOD was diluted with 20 mM Tris-HCl (pH 8.0) to a volume of 1.5 mL and concentrated to 200 μL. This process was repeated 10 times to produce $H1A_{IMD}$-NiSOD.

ESI-MS Analysis. To determine the MW of the NiSOD expression products, ESI-MS analysis was performed using a Bruker Esquire mass spectrometer equipped with an HP-HPLC instrument. Analysis was performed under protein denaturing conditions in 0.1% formic acid with the skimmer voltage set to 120 V, and samples were prepared to a final monomer concentration of 20 μM (Table 1).

Metal Analysis. A PerkinElmer Optima 4300 DV inductively coupled plasma-optical emission spectrometer was used to quantify the nickel content of the reconstituted mutant proteins. This instrument is equipped with a 40 MHz free-

DOI: 10.1021/bi501258u
Biochemistry 2015, 54, 1016−1027

running generator and a segmented-array charge-coupled device detector. The sample introduction system consisted of a concentric nebulizer with a cyclonic spray chamber. The concentration of nickel in each sample was determined at a λ of 231.604 nm.

Quaternary Structure and Stability. To determine the oligomeric state of the proteins, size-exclusion chromatography was performed using a Superdex 75 15/300 GL (GE Lifesciences) column. The column was standardized with albumin (67 kDa), ovalbumin (43 kDa), chymotrypsinogen (25 kDa), and ribonuclease A (13.7 kDa). A standard curve was constructed by plotting V_e/V_0 versus MW (where V_e is the elution volume of the peak and V_0 the elution volume of blue dextran), and the data were fit with a second-order polynomial. The apparent MW determined (Table 2) is in agreement with

Table 2. Size-Exclusion Chromatography

NiSOD sample	elution volume (mL)	MW (kDa)	corrected MW (kDa)	quaternary structure [calcd (kDa)]
WT	9.94	61.1	79.2	hexamer (79.2)
H1A-NiSOD	10.08	58.9	76.5	hexamer (78.8)
R47A-NiSOD	9.97	61.0	78.6	hexamer (79.0)
	12.76	21.9	39.4	trimer (39.5)
E17A/R47A-NiSOD	9.98	60.8	78.3	hexamer (78.3)
	12.47	24.5	42.0	trimer (39.2)
E17R/R47E-NiSOD	10.06	59.3	76.8	hexamer (79.2)
	12.59	23.4	40.9	trimer (39.6)

calculated MW values based on the elution volume. Because NiSOD is a tightly organized hexamer of four-helix bundles, the protein is eluted at elution volumes lower than those typical for ~80 kDa proteins. The corrected MW corresponds to adjusted molecular values based on the known MW and elution volume of WT-NiSOD. WT-NiSOD and NiSOD variants were injected onto the column at a concentration of 480 μM (monomer) in 20 mM Tris and 100 mM NaCl (pH 8.0), and the retention volume of the peak(s) (V_e/V_0) from each chromatogram was analyzed using the standard curve to determine the molecular weights of the eluted proteins (see the inset of Figure 3).

Melting temperatures (T_m) were measured with a Microcal VP-DSC instrument with a 0.5 mL sample and reference cells. Samples were concentrated to 100−140 μM monomer in 50 mM Tris buffer. Protein samples and blank 50 mM Tris buffer were degassed under vacuum for 10 min and added via syringe to the cells using a pulsing motion to expel air bubbles. Samples were run at 30 psi over 25−100 °C at a scan rate of 30 °C/h. Baseline correction and normalization were performed with the Microcal interface to the Origin software package, and T_m values were taken to be the peak maxima of the thermogram.

Crystallography of H1A-NiSOD. Crystals of H1A-NiSOD were grown by hanging drop vapor diffusion as previously described.[13] Prior to cryo-cooling and data collection, the crystals were transferred into growth buffer supplemented with 40% glycerol. X-ray diffraction data (266 frames, 0.75 deg/frame) were collected at APS beamline X6A at a wavelength of 0.9184 Å. Data were integrated and merged in HKL2000[15] to a resolution of 2.01 Å. The structure was determined by Fourier synthesis using Protein Data Bank entry 3G4X. The structure

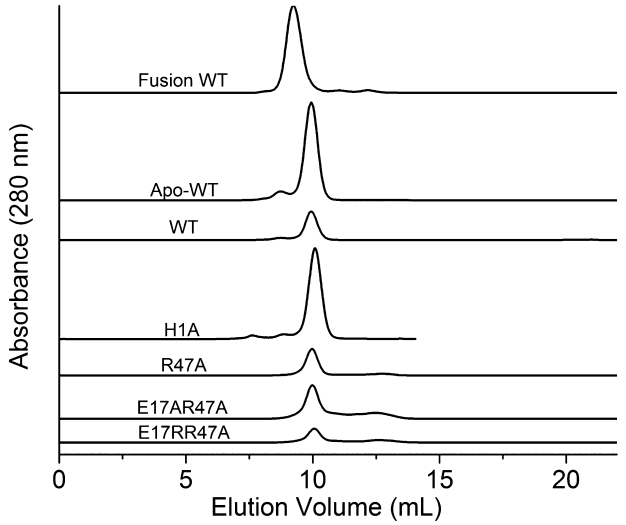

Figure 3. Size-exclusion chromatograms for WT-, H1A-, R47A-, E17A/R47A-, and E17R/R47E-NiSOD.

was refined in the CCP4 program Refmac[16] and built using Coot.[17]

To determine the nickel content of the crystals, a sample of the H1A-NiSOD crystals was dissolved in purified water and the protein concentration was determined using the absorbance at 280 nm. The sample was then diluted to a calculated concentration of 50 ppb based on nickel content determined by ICP-OES. Solution standards of nickel were made in purified water at concentrations of 1−500 ppb, and the H1A-NiSOD sample and nickel standards were analyzed by inductively coupled plasma mass spectrometry (ICP-MS) in triplicate.[18] The area under each peak was calculated, and a standard curve was constructed to back calculate the Ni concentration in the protein sample.

X-ray Absorption Spectroscopy. X-ray absorption spectroscopy (XAS) data collection and analysis were performed as previously described using a model that includes multiple scatterings from second-coordination sphere atoms in the chelate rings formed as a result of the bidentate coordination of His1 (N-terminal amine and imidazole side chain) and Cys2 (amidate and thiolate side chains).[13,14,19] Nickel K-edge XAS data were collected on beamline X3B (and X9B) at the National Synchrotron Light Source (Brookhaven National Laboratory, Upton, NY). Samples of frozen protein solutions [1−3 mM, based on nickel content, in 20 mM Tris-HCl (pH 8.0)] were placed in polycarbonate holders inserted into aluminum blocks and held near 50 K using a He displex cryostat. The ring conditions for data collection were 2.8 GeV and 120−300 mA. A sagittally focusing Si(111) double-crystal monochromator and a 13-channel Ge fluorescence detector (Canberra) were used for data collection. X-ray absorption near-edge spectroscopy (XANES) data were collected from ±200 eV relative to the nickel K-edge. The edge energy reported was taken to be the maximum of the first derivative of the XANES spectrum. Extended X-ray absorption fine structure (EXAFS) data were collected to 9307 eV (k = 16 Å^{-1}). The X-ray energy for the K-edge of nickel was internally calibrated to 8331.6 eV using transmission data from a nickel foil. The data shown are averages of five or six scans and were analyzed using the EXAFS123 software package for XANES data and the SixPack software package for EXAFS data.[20] Scattering

DOI: 10.1021/bi501258u
Biochemistry 2015, 54, 1016−1027

parameters for SixPack fitting were generated using the FEFF 8 software package.[21] The SixPack fitting software builds on the ifeffit program.[22] The coordinates of the oxidized and reduced NiSOD models obtained from DFT geometry optimizations were used as input files for FEFF 8.[11] Two sets of input files were used, one that included all non-hydrogen atoms from the **ox**[1] computational model and another that eliminated the apical imidazole ligand, as in the **red** model.[11] A comparison of the fits obtained using these two models was used to assess ligation by the His1 imidazole. To evaluate different models on the basis of a given data set, ifeffit uses three goodness of fit parameters, namely, χ^2 (eq 4), reduced χ^2, and the R factor (eq 5), where N_{idp} is the number of independent data points, N_{ε^2} is the number of uncertainties to minimize, $\mathrm{Re}(f_i)$ is the real part of the EXAFS fitting function, and $\mathrm{Im}(f_i)$ is the imaginary part of the EXAFS fitting function.

$$\chi^2 = \frac{N_{idp}}{N_{\varepsilon^2}} \sum_{i=1}^{N} \{[\mathrm{Re}(f_i)]^2 + [\mathrm{Im}(f_i)]^2\} \quad (4)$$

The reduced $\chi^2 = \chi^2/(N_{ind} - N_{varys})$ (where N_{varys} is the number of refining parameters) and represents the degrees of freedom in the fit. The R factor for the fit (eq 5) is scaled to the magnitude of the data, making it proportional to χ^2. To compare different models (fits), the R factor and reduced χ^2 parameters can be evaluated to determine which model provides the best fit, in which case both parameters should be minimized. Although the R factor will always improve with an increasing number of adjustable parameters, reduced χ^2 will go through a minimum and then increase, indicating that the model is overfitting the data.

$$R = \frac{\sum_{i=1}^{N} \{[\mathrm{Re}(f_i)]^2 + [\mathrm{Im}(f_i)]^2\}}{\sum_{i=1}^{N} \{[\mathrm{Re}(\tilde{\chi}\,\mathrm{data}_i)]^2 + [\mathrm{Im}(\tilde{\chi}\,\mathrm{data}_i)]^2\}} \quad (5)$$

EPR and Spin Quantification of As-Isolated, Dithionite-Reduced, and $IrCl_6$-Oxidized NiSOD Mutants. X-Band EPR spectra were obtained on a Bruker ELEXSYS E-500 X-band spectrometer. The data were collected over a 1500 G field centered at 3100 G with a modulation frequency of 100 kHz, a modulation amplitude of 10 G, and a time constant of 327 ms. The microwave power was set to 20 mW with a frequency of 9.58 GHz. To determine the fraction of Ni(III) centers present in each NiSOD variant, spin quantitation was performed by double integration of the EPR spectra, and the total concentration of Ni in each sample was determined using ICP-OES (λ = 231.604 nm). A 1.03 mM sample of $CuCl_2$ containing 1.3 mM EDTA was used as an EPR spin integration standard. Reduced samples were first treated with 10 molar equiv of sodium dithionite in an anaerobic environment and analyzed by EPR spectroscopy for the presence of Ni(III). The reduced samples were buffer exchanged anaerobically with fresh 20 mM Tris (pH 8.5) to remove excess reducing agent and treated with 2 molar equiv of $IrCl_6$ to produce the oxidized samples. The Ni(III) content in the oxidized samples was then determined by EPR spectroscopy.

Kinetics. Kinetic experiments used pulse radiolytic generation of $O_2^{\bullet-}$ and were conducted using a 2 MeV Van de Graaff accelerator at Brookhaven National Laboratory, as previously described.[13,14] Superoxide radicals were generated upon pulse radiolysis of an aqueous, air/O_2-saturated solution containing 10 mM phosphate, 30 mM formate, and 5 μM ethylenediaminetetraacetic acid (EDTA). Catalytic rate constants were obtained by monitoring the disappearance of $O_2^{\bullet-}$ at 260 nm in the presence of micromolar concentrations of mutant NiSOD. The path length of the quartz cell used was 2.0 cm, and a 100−700 ns pulse width was chosen, resulting in the generation of 1−7 μM $O_2^{\bullet-}$ per pulse. The reported rate constants are based on metal concentration, with the assumption that all nickel ions are specifically bound and equally contributing to $O_2^{\bullet-}$ dismutation.

The transient species observed for WT- and H1A-NiSOD were characterized by recording the absorption as a function of wavelength during pulses from the Van de Graaff accelerator. The extinction coefficients were calculated using a simple bimolecular mechanism for the formation of the absorbing species [e.g., O_2^- + H1A-Ni(II)SOD], and the extinction coefficient of the transient species was calculated assuming a first-order process for the disappearance of the absorbing species. Data were collected at 80 μM H1A-NiSOD.

RESULTS

Protein Characterization. All of the expressed fusion proteins had the expected MWs for the intended single- and double-amino acid substitutions as verified by ESI-MS (Table 1). Upon reconstitution of proteins processed to remove the N-terminal extension, each of the mutant proteins bound nickel at varying Ni:monomer ratios that were <1:1, using the same method for removing excess and nonspecifically bound Ni(II) (*vide supra*) (Table 1). For WT-NiSOD and E17A/R47A-NiSOD, the Ni:monomer ratio was ∼0.9, close to 1:1. The other mutants had a lower Ni content, ranging from 0.6 for R47A-NiSOD to 0.19 for H1A-NiSOD. Unlike the native enzyme, which is golden brown in color due to S(Cys) → Ni(III) charge transfer (LMCT) transitions near 380 nm, the H1A-NiSOD and E17A/R47A-NiSOD mutants were a lighter tan color. This difference likely results from the lower nickel loading and because all or most of the nickel centers are in the reduced, Ni(II), state in these variants (*vide infra*). Size-exclusion chromatography (SEC) data of the reconstituted NiSOD variants exhibited an elution peak with a retention volume corresponding to the molecular weights appropriate for homohexamers, as is the case for WT-NiSOD (Table 2 and Figure 3). In addition, the SEC data for the H-bonding mutants, R47A-, E17R/R47A-, and E17A/R47A-NiSOD, showed small peaks that are consistent with estimated MWs close to those calculated for trimers, suggesting that perturbations of the H-bonding network weaken the "dimer of trimers" hexameric structure.

The overall protein thermal stability was altered by the amino acid substitutions as revealed by the DSC data. Specifically, the variants generally have melting temperatures (T_m) 10−20 °C lower than those of WT-NiSOD (Table 1 and Figure 4) and form homohexamers less stable than those of WT-NiSOD. The DSC thermogram of WT-NiSOD exhibits an asymmetric curve, suggesting a complex thermal denaturation of the protein (Figure 4).[13,14] A likely interpretation is that the lower-temperature tail represents dissociations of the hexamer, while the sharp transition represents unfolding of the helical subunits. This hypothesis is supported by the fact that WT-NiSOD and the R47A-NiSOD variant, which contain an intersubunit His1−Glu17 H-bond, show pronounced tailing, whereas the variants lacking this H-bond (or the apical His imidazole altogether) exhibit a more symmetrical peak, consistent with a more labile hexamer due to the loss of the

DOI: 10.1021/bi501258u
Biochemistry 2015, 54, 1016−1027

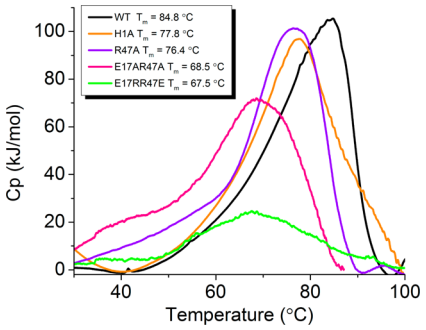

Figure 4. DSC thermograms of H1A-, R47A-, E17A/R47A-, and E17R/R47E-NiSOD compared with that of WT-NiSOD.

intersubunit H-bond. This interpretation is also consistent with the SEC data (*vide supra*).

Electron Paramagnetic Resonance. Amino acid substitutions that alter the active site H-bonding network present in WT-NiSOD affect the oxidation state and/or redox potential of the nickel site, as revealed by EPR spectra of the variant proteins. Resting (as-isolated) native and recombinant WT-NiSOD exhibit a rhombic EPR spectrum that arises from a five-coordinate, low-spin ($S = {}^1/_2$) Ni(III) center, with the unpaired electron residing in the Ni $3d_{z^2}$-based molecular orbital (MO). In addition, the spectrum reveals N-hyperfine structure on the high-field component that arises from coordination of the apical His1 imidazole ligand. Spin quantitation indicates that the EPR signal intensity accounts for only half of the nickel atoms in the sample; therefore, as-isolated WT-NiSOD is approximately half-oxidized and half-reduced.[13] As-isolated R47A-NiSOD and E17R/R47E-NiSOD display EPR signals with lower intensities that are very similar to those of the WT-NiSOD Ni(III) signals (Figure 5), including the N-hyperfine structure, indicating that the Ni(III) species retain the His-on structure. As-isolated H1A-NiSOD and E17A/R47A-NiSOD as well as reduced samples of R47A-NiSOD and E17R/R47E-NiSOD$_{red}$ lack this EPR spectrum; all are EPR-silent (data not shown), indicating that only Ni(II) is present. Double integration of the R47A-NiSOD and E17R/R47E-NiSOD EPR signals and comparison with the total Ni content of the samples, as determined by ICP-OES, indicate that the samples contain ~15 and 8% Ni(III), respectively. This result shows that a perturbation of the active site H-bonding network affects the redox potential of the Ni site and/or the stability of the WT-like oxidized Ni(III) active site structure. Treatment of reduced R47A-, E17A/R47A-, and E17R/R47E-NiSOD with the oxidant $IrCl_6$ did not result in an increase in EPR signal intensity.

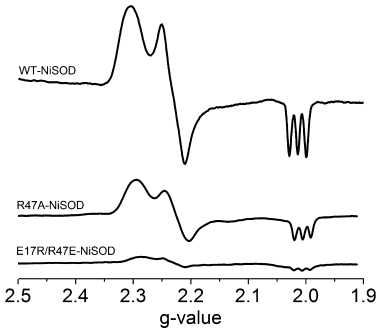

Figure 5. EPR spectra of WT-, R47A-, and E17R/R47E-NiSOD.

MCD. Variable-temperature variable-field MCD spectra were obtained as previously described.[11] Because of the low sample concentrations used, the signal-to-noise ratio of the spectra obtained is relatively low. However, the MCD data clearly show that the paramagnetic Ni(III) fraction varies from variant to variant (consistent with the EPR results presented here) and that the Ni(II) fraction is low-spin and diamagnetic, as in WT-NiSOD (see Figures SI-4–SI-6 of the Supporting Information).

X-ray Absorption Spectroscopy. X-ray absorption spectroscopy provides local structural information regarding the nickel sites. As such, structural information regarding the fraction of nickel-bound variants could be obtained even in cases where the portion of the protein comprising the "Ni-hook" motif was disordered in the crystal structures. However, such information represents an average of all of the nickel site structures in the sample. Nonetheless, XAS data of as-isolated WT-NiSOD [a 50:50 mixture of Ni(III) and Ni(II) centers] clearly contain features reflecting the coordination of the apical His1 imidazole that are lacking in the XAS data of reduced WT-NiSOD, where this ligand is not bound (Table 3 and Figure SI-2 of the Supporting Information).[23]

XANES. The XANES region of the nickel K-edge XAS spectrum (Figure 6) provides information about the nickel center coordination number and geometry and served as the basis for the geometry determination shown in Table 4. The spectrum obtained for H1A-NiSOD has a peak near 8331 eV that is associated with a Ni 1s → 3d electronic transition (Table 4), the area of which is consistent with a planar four-coordinate or pseudo-octahedral six-coordinate (centrosymmetric) nickel site.[24] The presence of a peak near 8336 eV associated with a Ni 1s → $4p_z$ electronic transition in the H1A-NiSOD spectrum is consistent with a planar four-coordinate geometry.[24]

An attempt to recover the WT-NiSOD structure by adding imidazole to the buffer did not produce the expected five-

Table 3. XANES and EXAFS Analysis of Dithionite-Reduced and As-Isolated WT-NiSOD Using the Proposed Fitting Model Utilizing Theoretical Coordinates from ox[1] When an Imidazole Is Included and red When an Imidazole Is Eliminated

sample	1s → 3d peak area (×10^2 eV)	geometry	N	R (Å)	σ^2 (×10^3 Å^{-2})	ΔE_0 (eV)	reduced χ^2	residual
native NiSOD[b]	1.2(7)	pl[c]	2N	1.87(3)	7(3)	1(2)	9.53	0.0311
dithionite-reduced NiSOD			2S	2.15(1)	1(1)			
WT-NiSOD[a]	3.5(9)	py[d]	2N	1.73(3)	1(1)	−14(7)	40.43	0.0267
as-isolated			1N	2.09(1)	1(12)			
			2S	2.18(6)	4(4)			
WT-NiSOD[b]			2N	1.74(6)	1(3)	−13(2)	77.32	0.0468
as-isolated			1N	1.9(2)	0(6)			
			2S	2.11(9)	4(4)			

[a]Fit includes one imidazole. [b]Fit includes zero imidazoles. [c]Planar. [d]Pyramidal.

DOI: 10.1021/bi501258u
Biochemistry 2015, 54, 1016–1027

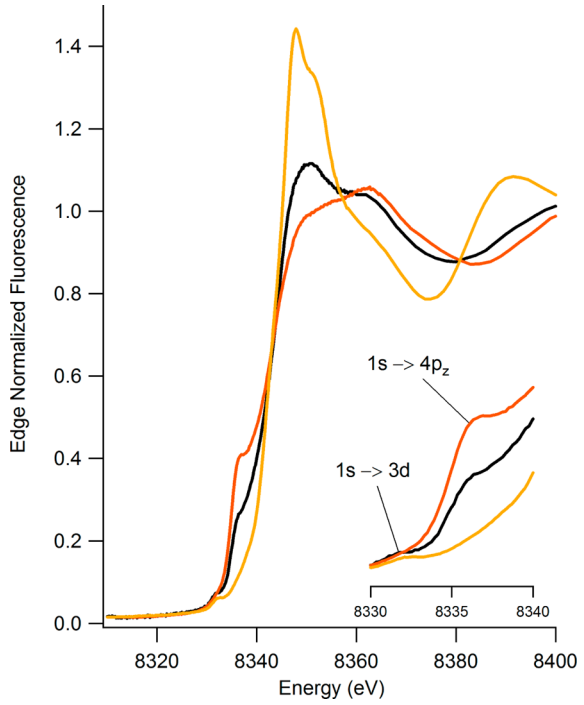

Figure 6. Ni K-edge XANES spectra for as-isolated WT-NiSOD (black), H1A-NiSOD (dark orange), and H1A$_{IMD}$-NiSOD (light orange). The inset shows the pre-edge region showing features associated with 1s → 3d and 1s → 4p$_z$ transitions.

coordinate pyramidal imidazole adduct. Instead, the XANES spectrum obtained for H1A$_{IMD}$-NiSOD is consistent with a six-coordinate Ni site. The spectrum features a peak near 8331 eV associated with a Ni 1s → 3d electronic transition (Table 4), the area of which is consistent with a centrosymmetric arrangement of ligands (i.e., a four- or six-coordinate nickel site), and the absence of a peak or shoulder near 8336 eV is consistent with a six-coordinate geometry.[24] Compared with those of WT-NiSOD, the XANES data for the H1A$_{IMD}$-NiSOD mutant also feature an increase in the white line region (0−50 eV above the edge) that is indicative of an increase in the ratio of N/O donors to S donors,[24] demonstrating that the addition of imidazole promotes a change in coordination at the active site.[12,13,23]

The XANES spectra obtained for the as-isolated H-bonding variants (Figure 8) R47A-, E17R/R47E-, and E17A/R47A-NiSOD have peaks near 8331 eV that are associated with a Ni 1s → 3d electronic transition, the intensities of which are consistent with the presence of a five-coordinate nickel site (Table 4).[24] Moreover, the presence of shoulders near 8336 eV in the R47A-, E17A/R47A-, and E17R/R47E-NiSOD spectra, which are associated with a Ni 1s → 4p$_z$ electronic transition, is consistent with a pyramidal five-coordinate geometry.[24]

EXAFS. The EXAFS region of the XAS spectrum provides information about the metal ligands, including the donor atom types, numbers, and bond distances. Analysis of the EXAFS features arising from atoms in the first coordination sphere (single-scattering analysis) indicates that the best fits for the

Table 4. XANES Analysis and Selected EXAFS Fits for the H-Bonding Variants of NiSOD

sample	edge energy (eV)	1s → 3d peak area (×10^2 eV)	geometry	N	R (Å)	σ^2 (×10^3 Å^{-2})	ΔE_0 (eV)	residual
H1A-NiSOD[b]	8342.8	0.7(2)	pl[d]	2N	1.91(3)	8(2)	5(2)	0.028
				2S	2.18(1)	4(1)		
H1A$_{IMD}$-NiSOD[a]	8344.6	2.9(6)	O$_h$	1N	1.89(6)	6(5)	5(3)	0.016
				3N	2.07(3)	3(2)		
				2S	2.28(3)	8(3)		
H1A$_{IMD}$-NiSOD[b]				1N	1.9(1)	8(12)	7(4)	0.033
				3N	2.08(4)	11(7)		
				2S	2.29(4)	9(7)		
H1A$_{IMD}$-NiSOD[c]				1N	1.81(3)	3(3)	2(2)	0.031
				3N	2.03(3)	4(2)		
				2S	2.25(2)	6(2)		
R47A-NiSOD[a]	8344.4	2.5(6)	py[e]	1N	2.19(7)	2(4)	11(7)	0.025
				2N	1.85(4)	5(2)		
				2S	2.16(1)	1(4)		
R47A-NiSOD[b]				1N	2.11(8)	0(10)	7(11)	0.040
				2N	1.87(4)	7(6)		
				2S	2.16(8)	2(2)		
E17A/R47A-NiSOD[a]	8343.6	1.4(6)	py[e]	1N	1.97(5)	0(3)	1(4)	0.037
				2N	1.81(3)	4(1)		
				2S	2.19(2)	4(2)		
E17A/R47A-NiSOD[b]				1N	1.95(7)	1(6)	2(5)	0.038
				2N	1.79(4)	3(2)		
				2S	2.18(2)	3(1)		
E17R/R47E-NiSOD[a]	8343.6	3.2(7)	py[e]	1N	2.12(3)	0(2)	9(7)	0.089
				2N	1.82(4)	4(2)		
				2S	2.14(4)	2(8)		
E17R/R47E-NiSOD[b]				1N	2.08(3)	0(9)	4(9)	0.072
				2N	1.83(5)	5(3)		
				2S	2.15(3)	4(12)		

[a]Fit includes one imidazole. [b]Fit includes zero imidazoles. [c]Fit includes two imidazoles. [d]Planar. [e]Pyramidal.

DOI: 10.1021/bi501258u
Biochemistry 2015, 54, 1016−1027

H1A-NiSOD and reduced H-bonding variants feature an N_2S_2 ligand-donor atom set that is consistent with the XANES results indicating a planar four-coordinate nickel site (Tables SI-2, SI-5, SI-7, and SI-9 of the Supporting Information). Single-scattering analysis of EXAFS data obtained for as-isolated R47A-, E17A/R47A-, and E17R/R47E-NiSOD indicates that the Ni sites associated with these variants feature N_3S_2 ligand-donor atom sets, which is consistent with the XANES results that indicate a pyramidal five-coordinate nickel site (Tables SI-4, SI-6, and SI-8 of the Supporting Information). Because signatures characteristic of S-donor ligands are present in the EXAFS spectra of all the NiSOD variants, the EXAFS spectra indicate that the nickel cofactor is binding in the same "Ni-hook" domain involving both Cys residues, as in WT-NiSOD. (The NiSOD sequence contains only three S-donor ligands, Cys2, Cys6, and Met28, and mutation of Met28 has no effect on the WT-NiSOD active site properties.)

Multiple-scattering analysis that includes data from scattering atoms in the second and third coordination spheres of the nickel center supports the presence of one imidazole ligand in the as-isolated H-bonding variants, consistent with nickel binding to the His1 imidazole, and shows no imidazole ligand for H1A-NiSOD, consistent with the loss of the apical His1 ligand. Table 4, Figure 7, and Figure 9 compare the best fits obtained for all NiSOD variants with and without paths derived from imidazole binding (second-coordination sphere C and third-coordination sphere N and C atoms). These fits also include the main chain carbon atoms from His1 and Cys2, which are involved in five-member chelate rings and are thus

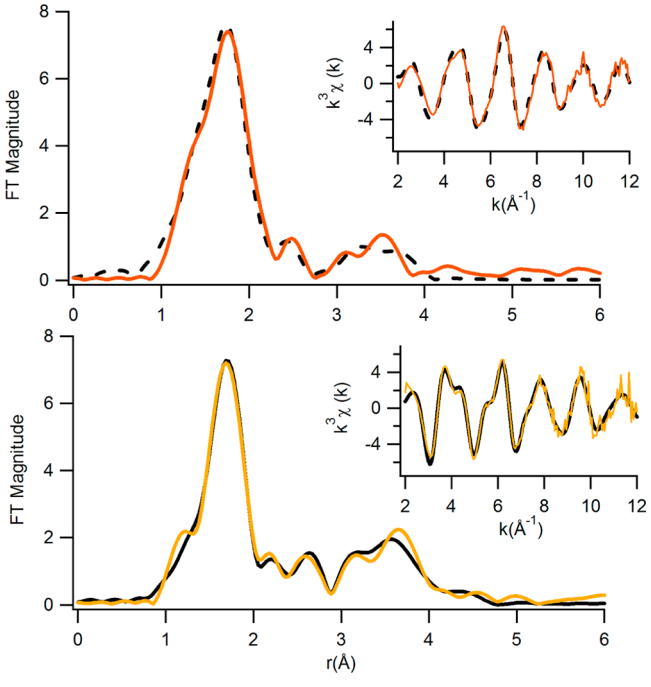

Figure 7. EXAFS spectra (colored lines) and best fits (black lines) from Table 4 for H1A-NiSOD (dark orange) and $H1A_{IMD}$-NiSOD (light orange). Dashed lines indicate fits generated without an imidazole ligand, and solid lines correspond to fits including one imidazole ligand. The fitting procedure including coordinates from the **red** theoretical calculation was applied when no imidazole was present, and the fitting procedure including coordinates from the **ox**[1] theoretical calculation was applied when an imidazole was present in the fit.

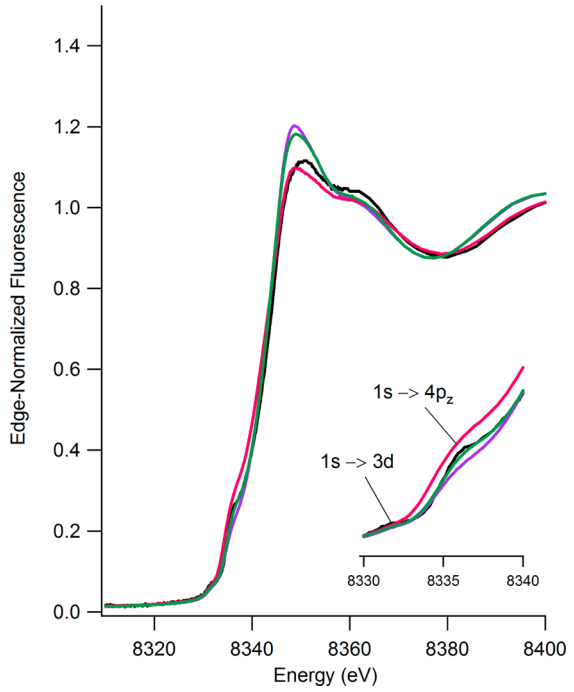

Figure 8. Ni K-edge XANES spectra for as-isolated WT-NiSOD (black), R47A-NiSOD (purple), E17A/R47A-NiSOD (pink), and E17R/R47E-NiSOD (green). The inset shows the pre-edge region showing features associated with 1s → 3d and 1s → $4p_z$ transitions.

held at specific distances that are similar to those involving the second-coordination sphere imidazole C atoms. The best fits for the Ni sites in the as-isolated mutant proteins were invariably those that included an imidazole ligand.

Crystal Structure of H1A-NiSOD. The X-ray crystallographic structure of H1A-NiSOD shows that the N-terminal region from residue 1 to 7 is disordered despite the spectroscopic observation that the metal is bound in the active site. Overall, the structure of H1A-NiSOD resembles that of apo-WT-NiSOD where the N-terminus is unresolved. The H1A-NiSOD crystals contained a nickel:protein ratio of 0.13:1, in close agreement with those of samples prepared as solutions for DSC, EPR, and XAS analysis. Collectively, these results suggest that while nickel binds to the N-terminal region of H1A-NiSOD, the metal binding region is highly mobile compared to that of nickel-bound WT-NiSOD.

Kinetics. The rates of superoxide dismutation by the variants with altered H-bonding interactions in the active site were determined by monitoring the disappearance of the optical absorption feature of pulse-radiolytically generated superoxide at 260 nm, in the presence and absence of the NiSOD mutant proteins. The catalytic rate observed for WT-NiSOD at pH 7.5 is 0.55×10^9 M^{-1} s^{-1},[13] as determined by the first-order disappearance of superoxide, is proportional to the NiSOD concentration, and displays a pH-independent catalytic rate over the pH range of approximately 6−10, indicating that the protons required to produce H_2O_2 are derived from the protein rather than bulk solvent (Figure 10). In contrast, the mechanism for spontaneous superoxide disproportionation is second-order in $[O_2^{\bullet-}]$, is highly pH-dependent, and proceeds at a rate of $\sim 2 \times 10^5$ M^{-1} s^{-1} at pH 7 under the conditions used here.[23,25] The disappearance of superoxide in the presence of all the variants displayed a rate that was proportional to enzyme concentration and pH-independent, indicating that these

DOI: 10.1021/bi501258u
Biochemistry 2015, 54, 1016−1027

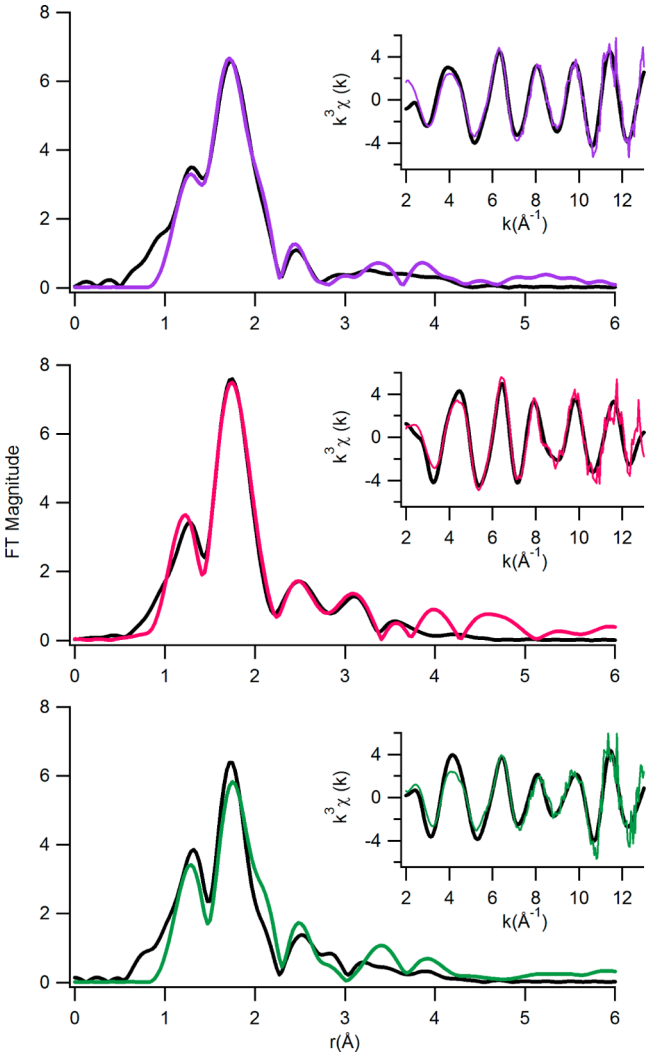

Figure 9. EXAFS spectra (colored lines) and fits (black lines) from Table 4 for R47A-NiSOD (purple), E17A/R47A-NiSOD (pink), and E17R/R47E-NiSOD (green). The fitting procedure including coordinates from the **ox**[1] theoretical calculation was applied when an imidazole was present in the fit.

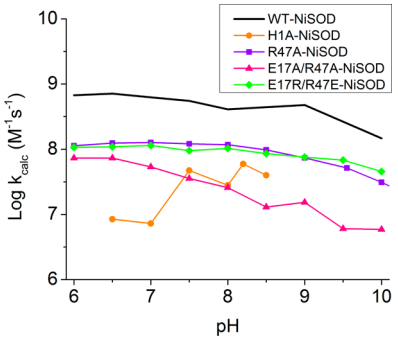

Figure 10. Dependence of k_{cat} on pH for WT-, H1A-, R47A-, E17A/R47A-, and E17R/R47E-NiSOD. Conditions: 4 μM H1A-NiSOD, 30 mM formate, 10 mM phosphate, and 5 μM EDTA.

variants are SODs and catalyze superoxide dismutation according to a common mechanism (Table 1 and Figure 10). In the case of H1A- and E17A/R47A-NiSOD (variants lacking a His1−Glu17 H-bond), the catalytic rate of superoxide dismutation is reduced by a factor of >10 compared to that of WT-NiSOD, and the presence of imidazole in the H1A$_{IMD}$-NiSOD sample did not restore activity. For R47A- and E17R/R47E-NiSOD, the catalytic rate of superoxide dismutation is reduced by a factor of ∼5 (Table 1 and Figure 10). This level of activity is between that observed for WT-NiSOD and H1A-NiSOD and indicates that variants that retain a possible His1−Glu17 H-bond are more active than those that lack this interaction but are still impeded by the structural effects of the amino acid substitutions.

Electronic absorption spectral data taken during the single turnover of as-isolated H1A-NiSOD with $O_2^{\bullet-}$ show evidence of the formation of species that are not observed for WT-NiSOD. Spectra obtained after reacting reduced WT-NiSOD with $O_2^{\bullet-}$ show the rapid appearance of an absorption feature near 380 nm that persists and has been assigned to a S → Ni(III) charge transfer transition,[11] consistent with the formation of stable Ni(III) sites. In contrast, the spectrum obtained for as-isolated H1A-NiSOD [Ni(II)] shows a rapid increase in absorbance near 390 nm, followed by a slow decay (much slower than catalysis) that is independent of [$O_2^{\bullet-}$] and occurs in two steps (k values of 40 and 3 s^{-1}) and thus involves a process and a transient species that are not observed for WT-NiSOD (Figure 11). The data are consistent with the formation

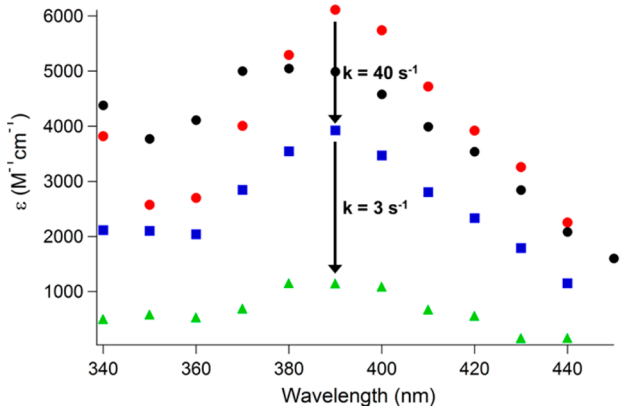

Figure 11. Spectral data taken during the reaction of WT-NiSOD (black) and H1A-NiSOD (red, blue, and green) with pulse-radiolytically generated $O_2^{\bullet-}$. Conditions: 80 μM H1A-NiSOD, 30 mM formate, 10 mM phosphate, and 5 μM EDTA.

of a distinct Ni(III) species, and its subsequent decay by a process that is independent of [$O_2^{\bullet-}$] suggests an internal redox process. The nature of the observed species awaits further spectroscopic investigation.

DISCUSSION

High-resolution crystal structures of WT-NiSOD reveal the presence of a H-bonding network formed between the NH group of the apical imidazole ligand from His1 and the Glu17 carboxylate from a neighboring subunit related by a 2-fold axis of rotation in the hexamer (Figure 2).[9,10] This interaction is supported by another intrasubunit H-bond between Glu17 and Arg47. In this study, four NiSOD mutant proteins were produced to experimentally evaluate the roles of the intersubunit H-bonding network involving the apical His1 imidazole ligand and Glu17 and Arg47 and to test the predictions made on the basis of previous DFT calculations.[11] H1A-NiSOD lacks the apical imidazole ligand and is thus related to the **red** and **ox-His$_{off}$** computational models. E17A/

DOI: 10.1021/bi501258u
Biochemistry 2015, 54, 1016−1027

R47A-NiSOD or E17R/R47E-NiSOD removes all the H-bonds or just the Glu17···His1 H-bond, respectively, and may be compared with the **ox**[1] model, which lacks the Glu17···His1 H-bond. R47A-NiSOD removes the Arg47···Glu17 intrasubunit H-bond, while retaining the Glu17···His1 intersubunit H-bond, and is comparable to the **ox**[3] model. Finally, the WT-NiSOD structure that includes the complete active site H-bonding network is best approximated by the **ox**[2] model. The computational results indicate that this Ni−NHis1$_{imidazole}$ interaction is important with respect to the electronic structure of the Ni(III) site by promoting nickel-centered rather than S-centered redox chemistry. They further revealed that the Ni−NHis1$_{imidazole}$ interaction is optimally tuned by the H-bonding network to adjust the energy of the redox active Ni $3d_{z^2}$ orbital and thus to fine-tune the redox potential of the site.

The **ox**[2] and **red** models reproduced the equatorial ligand distances for the nickel sites within 0.05 Å upon their comparison to the crystallographic distances.[11] However, a large discrepancy was noted between the DFT-optimized and crystallographically derived Ni−NHis1$_{imidazole}$ bond distances. In the **ox**[2] model, this distance is 2.14 Å, much shorter than the distance observed in the crystal structures of the Ni(III)-bound active sites (~2.3 Å). Analysis of the EXAFS spectra for Ni−L distances for low-spin Ni(II) sites in NiSODs reveals that the basal ligands contribute short Ni−N and Ni−S distances of ~1.9 and ~2.2 Å, respectively, as seen for dithionite-reduced WT-NiSOD (Tables 3). Using the protocol described above, and via comparison of fits with and without multiple scatterings from an imidazole ligand, the Ni−N$_{imidazole}$ distance in WT-NiSOD was determined to be 2.09(1) Å (Table 3), in reasonable agreement with the DFT-optimized value.

H1A-NiSOD. In addition to preventing coordination of imidazole to the oxidized Ni(III) site, the loss of the apical imidazole has a dramatic effect on the formation of the "Ni-hook" motif. In the crystal structure of H1A-NiSOD, the N-terminal residues prior to Val8 are disordered, suggesting that the H-bond between His1 and Glu17 plays a critical role in defining the structure of the NiSOD active site, because all of the ligands required to support coordination of the Ni(II) site structure are present. Analysis of the XAS spectrum of H1A-NiSOD confirms the presence of low-spin Ni(II) at the active site [EXAFS, 2Ni−N = 1.91(3) Å, and 2Ni−S = 2.18(1) Å (Table 4)], indicating metal binding to a planar four-coordinate N_2S_2 ligand environment as established here for dithionite-reduced WT-NiSOD using the protocol described above [2Ni−N = 1.87(3) Å, and 2Ni−S = 2.15(1) Å (Table 3)] or previously [2Ni−N = 1.91(1) Å, and 2Ni−S = 2.16(1) Å].[23]

Previous crystallographic results revealed that the Glu17···His1 H-bond is maintained in the structures of both oxidized [Ni(III)-bound] and reduced [Ni(II)-bound] WT-NiSOD,[9,10] but loss of the H-bond in H1A-NiSOD results in a disorder similar to that observed for the apoenzyme. The disorder observed in the apoenzyme was interpreted as indicating that the nickel binding to the active site ligands was required for stabilizing the structure of the "Ni-hook" motif. The loss of the "Ni-hook" structure observed for H1A-NiSOD indicates that the His1···Glu17 H-bond plays an essential role in stabilizing the structure of this motif and is consistent with the failure of chemical rescue of this variant. The XAS data show that the addition of imidazole to solutions of H1A-NiSOD produces a six-coordinate complex that features either one or two imidazole ligands but fails to lead to either the WT-NiSOD "Ni-hook" structure or increased catalytic activity (*vide infra*). Similarly, chemical rescue of H1A$_{IMD}$-NiSOD does not recover the WT-NiSOD EPR signal, and the active site remains in the Ni(II) oxidation state. Equilibria between planar four-coordinate complexes and six-coordinate complexes are common in Ni(II) coordination chemistry:

$$Ni(II)L_4 + L \Leftrightarrow Ni(II)L_5 \quad (6)$$

$$Ni(II)L_5 + L \Leftrightarrow Ni(II)L_6 \quad (7)$$

A five-coordinate intermediate is often not observed because the five-coordinate ⇔ six-coordinate equilibrium lies further to the right than the four-coordinate ⇔ five-coordinate equilibrium. Thus, one apparent function of the His1···Glu17 H-bond is to fold the "Ni-hook" in a way that prevents the formation of a six-coordinate Ni(II) site. Although the active site is near the surface of WT-NiSOD, it is effectively protected from solvent access by the hook motif. In the properly configured "Ni-hook", Val8 blocks access to the sixth coordination position, opposite to the imidazole side chain of His1. This would not be the case in the more mobile "Ni-hook" observed for H1A-NiSOD.

The four-coordinate ⇔ six-coordinate equilibrium would also alter the electronic properties of the active site, implying the conversion of a low-spin Ni(II) ion to a high-spin Ni(II) ion because six-coordinate Ni(II) centers are invariably high-spin.[26] The EXAFS analysis of H1A$_{IMD}$-NiSOD shows elongated M−L distances that support this proposal, in particular a Ni−S distance of 2.28(3) Å [~0.1 Å longer than the low-spin distance (Table 4)]. Such high-spin Ni(II) centers have also been observed in Cys-to-Ser mutants of NiSOD, which are catalytically inactive.[14,27] The formation of a high-spin, six-coordinate complex for the disordered "Ni-hook" domain may also sterically prevent folding into the "Ni-hook" structure that features a His1 imidazole···Glu17 H-bond, offering a possible explanation for why exogenous imidazole does not compensate for the loss of the His1 imidazole ligand.

Analysis of the kinetic data reveals that while H1A-NiSOD retains only ~4% of WT-NiSOD activity at pH 7.5, it remains an SOD catalyst, implying that a one-electron oxidized state is still accessible. The computed electronic structure for the **ox-His$_{off}$** model indicated that in the absence of the apical imidazole ligand Ni(II)SOD oxidation becomes a ligand-centered process,[11] offering a possible explanation for the instability of the oxidation product of H1A-NiSOD observed by spectroscopy. Specifically, the Ni(III) species formed by oxidation of H1A-NiSOD with $O_2^{\bullet-}$ may decay via reduction of the Ni(III) center by the thiolate ligands, a scenario that is also consistent with the lack of kinetic dependence on $[O_2^{\bullet-}]$.

H-Bonding Variants. Three additional NiSOD variants were designed to preserve the apical imidazole ligand but perturb the active site H-bonding network in various ways. Qualitative analyses of the Ni K-edge EXAFS spectra from a number of NiSOD samples have shown that the formation of a bond between the Ni ion and the His1 side chain results in two characteristic features in the Fourier-transform (FT) EXAFS spectrum that arise from the first-coordination sphere ligands, whereas in the absence of the apical ligand, only one broad feature is observed.[14] This presumably arises from the presence of a long Ni−N vector in samples with an apical imidazole ligand. This hypothesis is corroborated by the data obtained for oxidized and reduced WT-NiSOD, as well as for H1A-NiSOD, which has only one broad feature in the FT-EXAFS spectrum. Using this criterion, all of the mutant proteins featuring a

DOI: 10.1021/bi501258u
Biochemistry 2015, 54, 1016−1027

disrupted H-bonding network, but retaining the imidazole ligand, possess a Ni(II) ion that binds the apical imidazole in the as-isolated samples.

For R47A-NiSOD, the amino acid substitution removes the intrasubunit interaction between Glu17 and Arg47 but preserves the His1···Glu17 H-bond. According to the **ox**^{3} computational model, this is expected to increase the strength of the Glu17···His1 H-bond and thus to result in a Ni−$N_{imidazole}$ distance longer than that in WT-NiSOD. The distance found by EXAFS analysis [2.19(7) Å (Table 4)] is in agreement with the prediction from the **ox**^{3} computational model (2.14 Å).[11] In the two remaining mutants, E17A/R47A- and E17R/R47E-NiSOD, the Glu17···His1 H-bond is absent and a short Ni−$N_{imidazole}$ bond is predicted by the **ox**^{1} model.[11] Although the FT-EXAFS spectra of both variants show the two peaks expected for coordination of the His1 imidazole group, and the best EXAFS fits obtained include the imidazole ligand, the improvement of the fits is not sufficient to make a clear case for the presence or absence of this ligand. It may be that there is a more significant fraction of Ni centers adopting the His-off structure in these samples relative to either WT-NiSOD or R47A-NiSOD. Nonetheless, the Ni−$N_{imidazole}$ distances obtained from EXAFS fits that include the imidazole ligand are shorter [1.97(5) and 2.12(3) Å, respectively (Table 4)] than for R47A-NiSOD.

In addition to the structural effects observed for the H-bonding mutants, these species show perturbed catalytic activity that correlates with the intensity of their EPR signals. The sample that retains a Glu17···His1 H-bond, R47A-NiSOD, displays a 5-fold reduction in activity and ∼15% of the Ni ions in the as-isolated sample are in the Ni(III) state, compared with 50% for WT-NiSOD.[13] For E17R/R47E-NiSOD, the rate is reduced by a factor of ∼6, and our EPR data indicate that this variant contains ∼8% Ni(III). Lastly, in the case of E17A/R47A-NiSOD, the rate constant is reduced by a factor of >10 and the sample is EPR-silent [ruling out the presence of Ni(III)], as is the case for H1A-NiSOD. The correlation suggests that the variants have an impaired ability to access the oxidized, Ni(III) state for catalysis. This order also reflects the severity of the disruption to the H-bonding network (R47A-NiSOD < E17R/R47E-NiSOD < E17A/R47A-NiSOD and H1A-NiSOD) and points to the importance of the H-bonding network in the redox chemistry of the active site.

One possible explanation for the trend in activity of the NiSOD variants investigated is the one suggested by computational chemistry, namely, that changes in the Glu17···His1 H-bond affect the interaction between the apical imidazole ligand and the Ni(III) ion, resulting in a perturbation of the redox active Ni $3d_{z^2}$ orbital and thus perturbing the redox properties of the enzyme active site. This hypothesis is consistent with studies of small polypeptides that model the "Ni-hook" motif.[28−30] However, these models show a large H/D kinetic isotope effect[31] that is not observed in the WT-NiSOD enzyme, where the reaction rate is diffusion-limited, suggesting that the models catalyze superoxide disproportionation by a distinct mechanism. Nonetheless, the removal of the His imidazole ligand in the models affects the redox potential and activity in a way that is analogous to that of the H1A mutation; i.e., the complexes are isolated as Ni(II) species with planar N_2S_2 coordination, with increased redox potentials for the Ni(III/II) couple and reduced catalytic activity (by more than 1 order of magnitude).[28] Further, studies of model systems in which the imidazole ligand is modified, such as with N-Me, N-DNP, and N-Tos, show that the Lewis basicity of the ligand correlates with activity,[29,30] supporting the hypothesis that subtle electronic changes due to the H-bonding network involving the His1 donor are directly linked to optimizing the redox chemistry in the enzyme. However, on the basis of these studies, a loss of the Glu17···His1 H-bond should result in a stronger Ni−$N_{imidazole}$ interaction, a destabilized Ni $3d_{z^2}$ orbital, and a lower redox potential that favors Ni(III), which is counter to the impaired ability to access Ni(III) that is most consistent with the data for E17R/R47E- and E17A/R47A-NiSOD where the Glu17···His1 H-bond is missing. An alternative interpretation that is consistent with the XAS data is a two-state model in which the Ni(III) species represent a fraction of the protein that has a properly folded "Ni-hook" motif, and therefore a redox active nickel site, while the redox inactive fraction represents protein molecules with an unfolded "Ni-hook". This is more consistent with the data, because weakening the Glu17···His1 H-bond should favor a higher fraction in the unfolded and redox inactive state. Further, the fact that attempts to oxidize the Ni(II) center with $NaIrCl_6$ failed to increase the intensity of the Ni(III) EPR signals in the H-bonding mutants suggests that the low intensity of the EPR signal is not due solely to a minor perturbation of the redox potential and is more consistent with the "all-or-nothing" character of the two-state model.

■ ASSOCIATED CONTENT

Ⓢ Supporting Information

Eleven tables summarizing mutagenic primers used for mutant preparations, EXAFS fits used in analyzing the EXAFS data, crystallographic and MS-ICP nickel standards and calculated Ni contents for H1A crystals; six figures illustrating the XANES of dithionite-reduced native NiSOD and recombinant WT-NiSOD, EXAFS analysis of dithionite-reduced native NiSOD and recombinant WT-NiSOD, the standard curve of MS-ICP standards, and variable-temperature MCD spectra for E17A/R47A-NiSOD, E17R/R47E-NiSOD, and R47A-NiSOD. This material is available free of charge via the Internet at http://pubs.acs.org.

■ AUTHOR INFORMATION

Corresponding Author

*E-mail: mmaroney@chemistry.umass.edu. Phone: (413) 545-4876. Fax: (413) 545-4490.

Funding

This work was supported by grants from the National Science Foundation (CHE-0809188 to M.J.M.) and the National Institutes of Health (GM 64631 to T.C.B.).

Notes

The authors declare no competing financial interest.

■ ACKNOWLEDGMENTS

The U.S. Department of Energy, Division of Materials Sciences and Division of Chemical Sciences, supported XAS data collection at the National Synchrotron Light Source (NSLS) at Brookhaven National Laboratory. The National Institutes of Health supports beamline X3B (formerly X9B) at NSLS. Pulse radiolysis studies were conducted at the Center for Radiation Chemical Research, which is funded under U.S. Department of Energy Contract DE-AC02-98CH10886. We thank Ms. Carolyn Carr for help in preparing the figure graphics.

DOI: 10.1021/bi501258u
Biochemistry 2015, 54, 1016−1027

ABBREVIATIONS

BCA, bicinchoninic acid; cam, chloramphenicol; DFT, density functional theory; DSC, differential scanning calorimetry; DTT, dithiothreitol; EDTA, ethylenediaminetetraacetic acid; EPR, electron paramagnetic resonance; ESI-MS, electrospray ionization mass spectrometry; EXAFS, extended X-ray absorption fine structure; FPLC, fast protein liquid chromatography; ICP-OES, inductively coupled plasma-optical emission spectroscopy; IPTG, isopropyl β-D-1-thiogalactopyranoside; kan, kanamycin; LMCT, ligand to metal charge transfer; NTA, nitrilotriacetic acid; PCR, polymerase chain reaction; SDS–PAGE, sodium dodecyl sulfate–polyacrylamide gel electrophoresis; SEC, size-exclusion chromatography; SOD, superoxide dismutase; T_m, melting temperature; XANES, X-ray absorption near-edge structure; XAS, X-ray absorption spectroscopy.

REFERENCES

(1) Bielski, B. H., and Cabelli, D. E. (1991) Highlights of current research involving superoxide and perhydroxyl radicals in aqueous solutions. *Int. J. Radiat. Biol. 59*, 291–319.

(2) Bielski, B. H. J., Cabelli, D. E., Arudi, R. L., and Ross, A. B. (1985) Reactivity of HO_2/O_2 Radicals in Aqueous Solution. *J. Phys. Chem. Ref. Data 14*, 1041–1100.

(3) Valko, M., Rhodes, C. J., Moncol, J., Izakovic, M., and Mazur, M. (2006) Free radicals, metals and antioxidants in oxidative stress-induced cancer. *Chem.-Biol. Interact. 160*, 1–40.

(4) Sheng, Y., Abreu, I. A., Cabelli, D. E., Maroney, M. J., Miller, A.-F., Teixeira, M., and Valentine, J. S. (2014) Superoxide Dismutases and Superoxide Reductases. *Chem. Rev. 114*, 3854–3918.

(5) Miller, A. F. (2008) Redox tuning over almost 1 V in a structurally conserved active site: Lessons from Fe-containing superoxide dismutase. *Acc. Chem. Res. 41*, 501–510.

(6) Borgstahl, G. E. O., Parge, H. E., Hickey, M. J., Beyer, W. F., Hallewell, R. A., and Tainer, J. A. (1992) The Structure of Human Mitochondrial Manganese Superoxide-Dismutase Reveals a Novel Tetrameric Interface of 2 4-Helix Bundles. *Cell 71*, 107–118.

(7) Borgstahl, G. E. O., Pokross, M., Chehab, R., Sekher, A., and Snell, E. H. (2000) Cryo-trapping the six-coordinate, distorted-octahedral active site of manganese superoxide dismutase. *J. Mol. Biol. 296*, 951–959.

(8) Lah, M. S., Dixon, M. M., Pattridge, K. A., Stallings, W. C., Fee, J. A., and Ludwig, M. L. (1995) Structure-Function in *Escherichia coli* Iron Superoxide-Dismutase: Comparisons with the Manganese Enzyme from *Thermus thermophilus*. *Biochemistry 34*, 1646–1660.

(9) Barondeau, D. P., Kassmann, C. J., Bruns, C. K., Tainer, J. A., and Getzoff, E. D. (2004) Nickel superoxide dismutase structure and mechanism. *Biochemistry 43*, 8038–8047.

(10) Wuerges, J., Lee, J. W., Yim, Y. I., Yim, H. S., Kang, S. O., and Carugo, K. D. (2004) Crystal structure of nickel-containing superoxide dismutase reveals another type of active site. *Proc. Natl. Acad. Sci. U.S.A. 101*, 8569–8574.

(11) Fiedler, A. T., Bryngelson, P. A., Maroney, M. J., and Brunold, T. C. (2005) Spectroscopic and computational studies of Ni superoxide dismutase: Electronic structure contributions to enzymatic function. *J. Am. Chem. Soc. 127*, 5449–5462.

(12) Bryngelson, P. A., Arobo, S. E., Pinkham, J. L., Cabelli, D. E., and Maroney, M. J. (2004) Expression, reconstitution, and mutation of recombinant *Streptomyces coelicolor* NiSOD. *J. Am. Chem. Soc. 126*, 460–461.

(13) Herbst, R. W., Guce, A., Bryngelson, P. A., Higgins, K. A., Ryan, K. C., Cabelli, D. E., Garman, S. C., and Maroney, M. J. (2009) Role of conserved tyrosine residues in NiSOD catalysis: A case of convergent evolution. *Biochemistry 48*, 3354–3369.

(14) Ryan, K. C., Johnson, O. E., Cabelli, D. E., Brunold, T. C., and Maroney, M. J. (2010) Nickel superoxide dismutase: Structural and functional roles of Cys2 and Cys6. *JBIC, J. Biol. Inorg. Chem. 15*, 795–807.

(15) Otwinowski, Z., and Minor, W. (1997) Processing of X-ray diffraction data collected in oscillation mode. *Methods Enzymol. 276*, 307–326.

(16) Collaborative Computational Project, No. 4 (1994) The CCP4 suite: Programs for protein crystallography. *Acta Crystallogr. D50*, 760–763.

(17) Emsley, P., and Cowtan, K. (2004) Coot: Model-building tools for molecular graphics. *Acta Crystallogr. D60*, 2126–2132.

(18) Mahar, M., Tyson, J. F., Neubauer, K., and Grosser, Z. (2008) High throughput sample introduction system for the analysis of drinking waters and wastewaters by ICP-MS. *J. Anal. At. Spectrom. 23*, 1204–1213.

(19) Leitch, S., Bradley, M. J., Rowe, J. L., Chivers, P. T., and Maroney, M. J. (2007) Nickel-specific response in the transcriptional regulator, *Escherichia coli* NikR. *J. Am. Chem. Soc. 129*, 5085–5095.

(20) Padden, K. M., Krebs, J. F., MacBeth, C. E., Scarrow, R. C., and Borovik, A. S. (2001) Immobilized metal complexes in porous organic hosts: Development of a material for the selective and reversible binding of nitric oxide. *J. Am. Chem. Soc. 123*, 1072–1079.

(21) Webb, S. M. (2005) SIXpack: A graphical user interface for XAS analysis using IFEFFIT. *Phys. Scr.*, 1011–1014.

(22) Ankudinov, A. L., Ravel, B., Rehr, J. J., and Conradson, S. D. (1998) Real-space multiple-scattering calculation and interpretation of X-ray-absorption near-edge structure. *Phys. Rev. B 58*, 7565–7576.

(23) Choudhury, S. B., Lee, J. W., Davidson, G., Yim, Y. I., Bose, K., Sharma, M. L., Kang, S. O., Cabelli, D. E., and Maroney, M. J. (1999) Examination of the nickel site structure and reaction mechanism in *Streptomyces seoulensis* superoxide dismutase. *Biochemistry 38*, 3744–3752.

(24) Colpas, G. J., Kumar, M., Day, R. O., and Maroney, M. J. (1990) Structural Investigations of Nickel-Complexes with Nitrogen and Sulfur Donor Ligands. *Inorg. Chem. 29*, 4779–4788.

(25) Fridovich, I. (1998) Oxygen toxicity: A radical explanation. *J. Exp. Biol. 201*, 1203–1209.

(26) Melnik, M., Sramko, T., Dunajjurco, M., Sirota, A., Jona, E., and Holloway, C. E. (1994) Nickel Coordination-Compounds: Classification and Analysis of Crystallographic and Structural Data (Vol 14, Pg 1, 1994). *Rev. Inorg. Chem. 14* (1–4), 1–300.

(27) Johnson, O. E., Ryan, K. C., Maroney, M. J., and Brunold, T. C. (2010) Spectroscopic and computational investigation of three Cys-to-Ser mutants of nickel superoxide dismutase: Insight into the roles played by the Cys2 and Cys6 active-site residues. *JBIC, J. Biol. Inorg. Chem. 15*, 777–793.

(28) Neupane, K. P., Gearty, K., Francis, A., and Shearer, J. (2007) Probing variable axial ligation in nickel superoxide dismutase utilizing metallopeptide-based models: Insight into the superoxide disproportionation mechanism. *J. Am. Chem. Soc. 129*, 14605–14618.

(29) Shearer, J., and Long, L. M. (2006) A nickel superoxide dismutase maquette that reproduces the spectroscopic and functional properties of the metalloenzyme. *Inorg. Chem. 45*, 2358–2360.

(30) Shearer, J., Neupane, K. P., and Callan, P. E. (2009) Metallopeptide based mimics with substituted histidines approximate a key hydrogen bonding network in the metalloenzyme nickel superoxide dismutase. *Inorg. Chem. 48*, 10560–10571.

(31) Shearer, J. (2013) Use of a metallopeptide-based mimic provides evidence for a proton-coupled electron-transfer mechanism for superoxide reduction by nickel-containing superoxide dismutase. *Angew. Chem. 52*, 2569–2572.

DOI: 10.1021/bi501258u
Biochemistry 2015, 54, 1016–1027